ACS APPLIED MATERIALS & INTERFACES

Research Article

www.acsami.org

Amphiphilic Polyelectrolyte/Prodrug Nanoparticles Constructed by Synergetic Electrostatic and Hydrophobic Interactions with Cooperative pH-Sensitivity for Controlled Doxorubicin Delivery

Pingsheng Huang,[†,‡,§] Weiwei Wang,[†,⊥] Junhui Zhou,[‡] Fuli Zhao,[‡] Yumin Zhang,[∥] Jinjian Liu,[∥] Jianfeng Liu,[∥] Anjie Dong,[‡,§] Deling Kong,*[,⊥] and Jianhua Zhang*[,‡,§]

[‡]Department of Polymer Science and Technology and Key Laboratory of Systems Bioengineering of the Ministry of Education, School of Chemical Engineering and Technology, Tianjin University, Tianjin 300072, China

[§]Collaborative Innovation Center of Chemical Science and Engineering (Tianjin), Tianjin 300072, China

[⊥]Chinese Academy of Medical Science & Peking Union Medical College, Institute of Biomedical Engineering. Tianjin 300192, China

[∥]Tianjin Key Laboratory of Molecular Nuclear Medicine, Institute of Radiation Medicine, Chinese Academy of Medical Science & Peking Union Medical College, Tianjin 300192, China

Supporting Information

ABSTRACT: To achieve higher therapeutic efficiency with catabatic side effects, desirable nanocarriers should be designed to retain the loaded drug tightly during the systemic circulation, but release the drug rapidly and efficiently upon endocytosis by tumor cells. Herein, to achieve "off-on" controlled delivery of DOX, novel amphiphilic polyelectrolyte/prodrug nanoparticles (NPs) with cooperative pH-sensitivity were constructed via synergistic electrostatic and hydrophobic interactions between slightly positively charged methoxy polyethylene glycol-*b*-(poly(2-(diisopropylamino) ethyl methacrylate-*co*-aminopropyl methacrylamide) (PEDPA) copolymer and negatively charged *cis*-aconityl-doxorubicin (CAD) prodrug (termed as PEDPA/CAD NPs). With polymer-prodrug synergistic noncovalent interactions, the drug loading content of PEDPA/CAD NPs could be improved up to 12.6% with favorable serum stability, and significantly lowered the drug leakage to 2.5% within 24 h at pH 7.4. However, nearly 80% of encapsulated drug could be released at pH 5.0 within 12 h, due to the cooperative effects of the protonation of PDPA blocks resulting in quick disassembly of NPs and the rapid hydrolysis of cis-aconityl linkage leading to charge-reverse of CAD. Moreover, the results of fluorescent microscopy imaging and flow cytometry measurements exhibited that DOX could be recovered and released rapidly from PEDPA/CAD NPs upon endocytosis and then exert therapeutic action in the cell nucleus. Importantly, the PEDPA/CAD NPs exhibited significantly higher antitumor efficiency in vivo with reduced nonspecific toxicity to normal tissues in comparation with free DOX. In summary, the NPs designed in this work, constructed by synergistic electrostatic and hydrophobic interactions with cooperative pH-sensitivity, which potentially resolved the dilemma between systemic stability and rapid intracellular drug release, would provide a promising nanomedicine platform for cancer therapy.

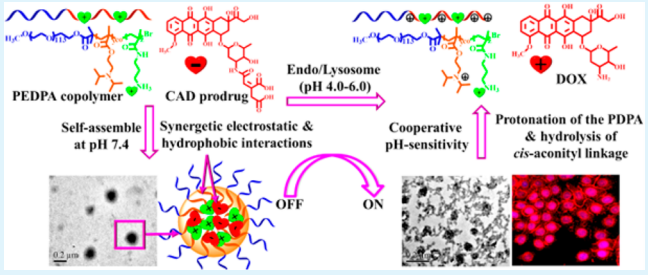

KEYWORDS: *pH-sensitive, nanoparticle, switchable delivery, doxorubicin, tumor treatment*

1. INTRODUCTION

Doxorubicin (DOX), a kind of FDA-approved anthracycline antibiotic, is clinically used in chemotherapy with a broad spectrum of antitumor activity.[1−3] However, its short systemic circulation time and undesirable biodistribution lead to not only poor therapeutic responses, but also intolerable side effects, especially the acute and accumulative cardiotoxicity.[4] Therefore, various polymeric nanocarriers have been fabricated to improve the treatment efficacy and safety of DOX, because of not only the flexibly modified structures, but also well-controlled compositions, shapes and properties.[5−9] Nevertheless, most traditional nanocarriers, which assembled mainly by coprecipitation of DOX with the hydrophobic blocks of amphiphilic copolymers, usually showed low drug loading content accompanied by an undesirable release profile.[10] Typically, the premature release led to drug loss in blood circulation that may result in severe side effects, whereas the slow intracellular drug release resulted in low drug bioavailability, which was insufficient to kill cancer cells and may cause multidrug resistance (MDR).[11,12]

So far, three major approaches have been explored to address this challenge. First, the incorporation of cross-linking structure

Received: February 1, 2015
Accepted: March 9, 2015
Published: March 9, 2015

DOI: 10.1021/acsami.5b00962
ACS Appl. Mater. Interfaces 2015, 7, 6340−6350

Scheme 1. Fabrication of DOX Delivery System via Synergetic Electrostatic and Hydrophobic Interactions with Cooperative pH-Sensitivity to Resolve the Dilemma between Systemic Stability and Intracellular Rapid Release

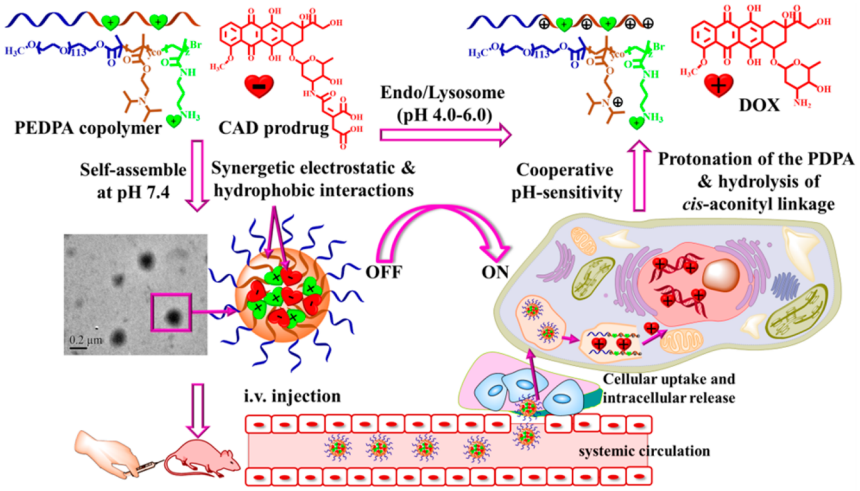

into polymeric NPs has proven to be a straightforward and feasible route to stabilize NPs and reduce the burst release. However, the drug release at the target sites was usually inhibited because of the low cooperativity between cross-linking structures and the hydrophobic core.[13−15] In addition, the incorporation of noncovalent interactions, such as $\pi-\pi$ stack,[16] electrostatic complexation,[17,18] and hydrogen bond,[19,20] have shown considerable value in the improvement of drug loading content and stability. However, the enhanced drug-hydrophobic block interactions usually exert a retardant effect on intracellular drug release. Another alternative way was the fabrication of micellar prodrugs, especially these with stimuli-responsive property based on the peculiar microenvironments of cancer cells, which were expected to combine the stability and cleavability to realize prolonged systemic circulation and appropriate intracellular drug release.[21−24] Nontheless, the drug release rate of many prodrug micelles was not always desirable, which could be attributed to not only low water availability in the hydrophobic core retarding the hydrolysis process but also the hydrophobic interaction between drug molecules and hydrophobic moiety hindering the drug diffusion.

Herein, to resolve the dilemma between systemic stability and intracellular rapid release, novel amphiphilic polyelectrolyte/prodrug nanoparticles (NPs) with cooperative pH-sensitivity were constructed via synergistic electrostatic and hydrophobic interactions between positively charged methoxy polyethylene glycol-*b*-(poly(2-(diisopropylamino) ethyl methacrylate-*co*-aminopropyl methacrylamide) (PEDPA) copolymers and negatively charged *cis*-aconityl-doxorubicin (CAD) prodrug (termed as PEDPA/CAD NPs). As illustrated in Scheme 1, because of the synergistic noncovalent interactions between PEDPA and CAD in the core of NPs, PEDPA/CAD NPs are expected to achieve high DOX-loading capacity with low premature leakage at physiological condition, whereas rapid release in the acidic endo/lysosomal compartments within tumor cells due to the combined effects of the protonation of PDPA block results in quick disassembly of NPs and the rapid hydrolysis of *cis*-aconityl linkage, leading to charge-reverse of CAD. Accordingly, the physicochemical characteristics and pH-sensitive release properties of PEDPA/CAD NPs were investigated in detail. The endocytosis and drug release behavior intracellularly was analyzed by flow cytometry measurement and fluorescent microscope imaging. The antitumor efficiency of PEDPA/CAD NPs was evaluated systematically in vitro and in vivo. The toxicity of PEDPA/CAD NPs, CAD and DOX against normal tissues was evaluated by histopathologic examinations

2. EXPERIMENTAL SECTION

2.1. Materials and Characterization. All the chemicals used in this work and the synthetic methods were demonstrated in the Supporting Information file.

To verify the chemical compositions of synthesized polymers and CAD prodrug, nuclear magnetic resonance (NMR) spectra were obtained on Varian Unity-Plus INOVA 500 using deuterated chloroform ($CDCl_3$) as the solvent. Gel permeation chromatography (GPC, Malvern, UK) installed with Viscotek GPCmax system was employed to analyze the molecular weight distribution (polydispersity index, PDI) of obtained copolymers, which was performed with a porous styrene divinylbenzene copolymer-based column (Org 300 × 7.8 mm, CLM3009, T6000M, General Mixed), using polystyrene as the standard material for calibration and THF as the mobile phase. The particle size, polydispersity index (PDI) and zeta potential of NPs in PBS solution (pH 7.4, 10 mM) were measured on Zetasizer (Malvern, 3000HS, UK) based on dynamic light scattering. The micromorphologies of all NPs were analyzed with transmission electron microscopy (TEM, Hitachi H600), during which the samples were prepared and viewed according to standard instructions.[25]

2.2. Preparation and Characterization of PEDPA and PEDPA/CAD NPs. In this study, the PEDPA/CAD NPs were prepared via nanoprecipitation methods. Subsequently, drug loading efficiency (DLE) and drug loading content (DLC) were measured by previous reported methods with some modifications.[20,25] The particle size, zeta potential, polydispersity index (PDI), and micromorphology of PEDPA NPs and PEDPA/CAD NPs were determined using Zetasizer and TEM. Furthermore, serum stability study of PEDPA/CAD NPs was also conducted according to a previously reported method.[9] The experimental details are given in the Supporting Information.

The fluorescence excitation spectrum of CAD and PEDPA/CAD NPs was measured by fluorescent spectrophotometer at 25 °C. The maximum absorption wavelength of CAD was used as the excitation wavelength which was detected by double beam UV−visible spectrophotometer (TU-1900, China).

2.3. In Vitro Cell Experiments. *2.3.1. Cell Culture.* In this experiment, HeLa and HepG2 cancer cells, mouse embryonic fibroblasts (3T3) cells, were cultured in 25 cm^2 tissue culture flasks, which was charged with penicillin (100 U/mL), 10% FBS, and streptomycin (100 U/mL). In addition, human acute monocytic

DOI: 10.1021/acsami.5b00962
ACS Appl. Mater. Interfaces 2015, 7, 6340−6350

Scheme 2. Synthetic Route of PEDPA Copolymers

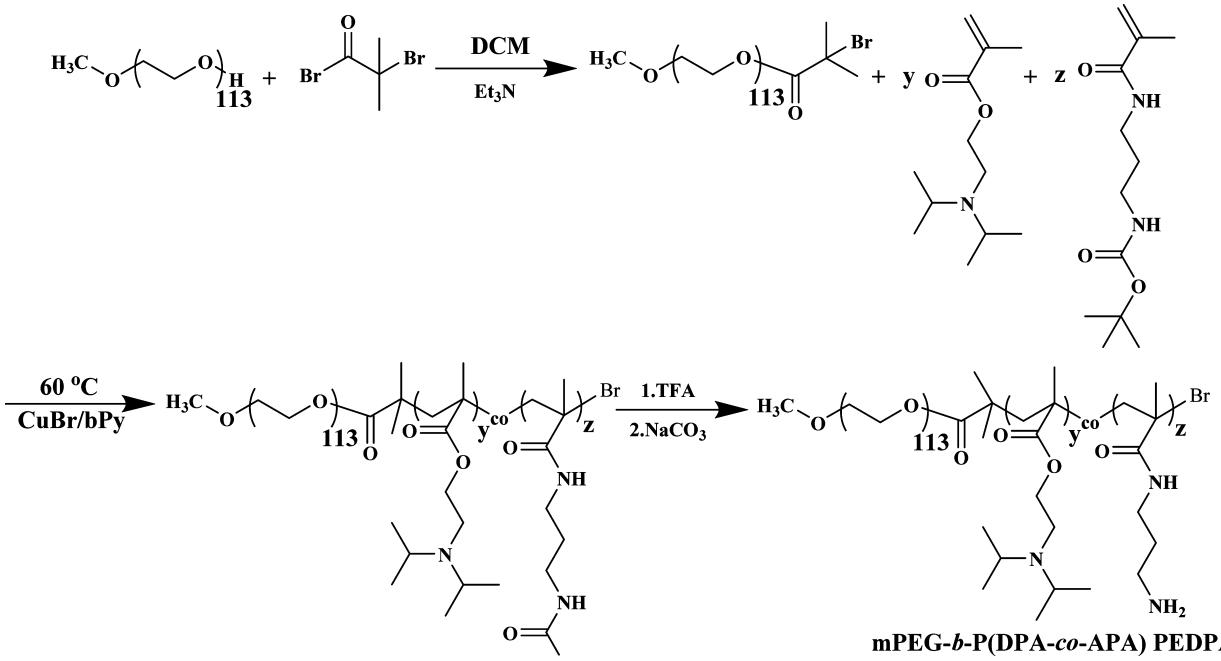

leukemia cell line (THP-1) was cultured in RPMI-1640 medium supplemented with 100 μg/mL streptomycin, 10% heat-inactivated fetal bovine serum, and 100 U/mL penicillin. All cell lines were maintained at 37 °C under standard cell culture conditions (5% CO_2 and 95% O_2).

2.3.2. Intracellular Drug Release Studies and Cytotoxicity Assay. HepG2 cells were used for the cellular uptake and intracellular drug release studies, which were performed on FACS Calibur flow cytometer (BD Biosciences, USA) and fluorescence microscopy (Leica AF 6500), respectively. In addition, the cytotoxicity evaluation was performed by MTT assay.[9,25,26]

Briefly, 24-well plates containing 0.5 mL of DMEM culture medium were seeded with HepG2 cells at density of 2×10^5 per well. After incubation for 24 h under standard culture conditions, formal medium was replaced with 0.5 mL fresh DMEM medium containing CAD, PEDPA/CAD NPs and free DOX. The drug concentration was 10 μg/mL. For the blank control, the medium was added with equal amount saline. After incubated for 4 h, the cells were washed by ice-cold PBS (pH 7.4) for three times, which were harvested through trypsin treatment. Subsequently, the harvested cells were resuspended in ice-cold PBS (pH 7.4) and subjected to centrifugation for 5 min at 1000 rpm at 4 °C. After treatment with centrifugation-wash for three cycles, fluorescence of cells was detected by flow cytometer.

The culture and treatment conditions of HepG2 cells for fluorescence microscopy imaging studies were same with that of flow cytometer measurements. Paraformaldehyde, dispersed in saline at concentration of 4%, was used to fix the cells. After incubation at 4 °C for 20 min, the cells were washed three times with cold PBS before counterstained with DAPI, which were observed on the fluorescence microscopy.

The cytotoxicity of free DOX, CAD, and PEDPA/CAD NPs against HepG2 cells and HeLa cells were evaluated by MTT assay. In addition, the cytocompatibility of blank PEDPA-3 NPs was evaluated not only on HepG2 cells and HeLa cells but also 3T3 cells and THP-1 cells. 96-well plates, which were supplemented with 100 μL of DMEM medium, were seeded with the above cells at a density of 5000 per well. After incubation for 24 h, 100 μL of fresh DMEM medium containing free DOX, CAD, PEDPA/CAD NPs, and blank PEDPA NPs replaced the original medium. After incubation for 48 h, the plates were resupplemented with 100 μL fresh medium. Subsequently, 25 μL of MTT PBS (pH 7.4, 10 mM) solution was added and incubated for 2 h. Then, 100 μL extraction buffer was added, followed by incubation overnight. The cells were then subjected to MTT assay, which was performed on a microplate reader according to previous methods.

2.6. In Vivo Animal Experiments. *2.6.1. Animal Subject and Tumor Models.* To investigate the tumor accumulation and antitumor efficacy, we purchased HepG2 tumor xenograft bearing female Balb/c nude mice (6–8 weeks old) from the Vital River Laboratory Animal Technology Co., Ltd. (Beijing, China). All animal experiments were conducted based on our previous reported methods, which were performed strictly according to the People's Republic of China national standard (GB/T 16886.6–1997).[9,25,26]

2.6.2. In Vivo Tumor Accumulation Investigation. Briefly, when the mean tumor size reached approximately 100 mm^3, CAD, DOX and PEDPA/CAD NPs were i.v. injected at dose of 5 mg/kg (n = 3). Saline was administered as the negative control. At predeterminate time intervals, tumor and major organs were harvested for ex vivo imaging, which were detected on the Kodak imaging system.

2.6.3. In Vivo Antitumor Efficacy Evaluation. The mice were divided into four treatment groups randomly (n = 13), when the mean tumor volume reached 100 mm^3 and this day was set as day 0. Mice were administered intravenously with free DOX, CAD, PEDPA/CAD NPs, and saline at dose of 5 mg DOX/kg body weight every 4 days. Tumor volume and body weight were measured every 2 days. The tumor inhibition study was stopped on the 20th day and the survival rate study was stopped on 34th day.

2.6.4. Histopathologic Evaluation. To evaluate the biosafety of the NPs formulations, we randomly sacrificed three mice in every group for pathologic analysis at the end of treatment (20th days, n = 3). The major organs including liver, spleen, heart, kidney, lung, and tumor were harvested immediately post dissection of these mice. The tissues and specimens were treated and obtained according to reported method, which were observed by optical microscope.[27]

3. RESULTS AND DISCUSSION

3.1. Synthesis and Characterization of PEDPA Copolymers. In this work, PEDPA copolymers were obtained in three steps (as illustrated in Scheme 2). First, the ATRP macroinitiator mPEG-Br was synthesized according to our previous reported method and characterized by ^1H NMR (shown in Figure S1 in the Supporting Information).[28] Then, mPEG-*b*-P (DPA-*co*-Boc-APA) was synthesized via ATRP using bPy and CuBr as the catalytic system under no oxygen

DOI: 10.1021/acsami.5b00962
ACS Appl. Mater. Interfaces 2015, 7, 6340–6350

Table 1. Characterization of PEDPA Copolymers

samples	DPA[a]	APA[a]	DPA[b]	APA[b]	Mn (Da)[b]	M_w/M_n[c]	CMC[d]
PEDPA-0	50	0	48	0	15388	1.29	1.05×10^{-4}
PEDPA-1	50	5	49	4	16169	1.25	1.99×10^{-4}
PEDPA-2	50	10	47	8	16312	1.27	3.16×10^{-4}
PEDPA-3	50	15	47	13	17023	1.33	7.01×10^{-4}

[a]The feeding ratio of two monomers. [b]Calculated from ^{1}HNMR. [c]Determined by GPC. [d]Measured by pyrene-based fluorescent spectrometry.

conditions. Subsequently, the deprotection of Boc was rapidly accomplished using 5 equiv of TFA in THF, and the amino group was then obtained by desalination using excessive sodium carbonate.

The molecular weight distribution and chemical compositions of PEDPA copolymers were evaluated by GPC and ^{1}H NMR, respectively (as shown in Table 1). All characteristic signals of mPEG, DPA, Boc-APA and APA units could be seen clearly in Figure 1. Herein, the molecular weight of mPEG

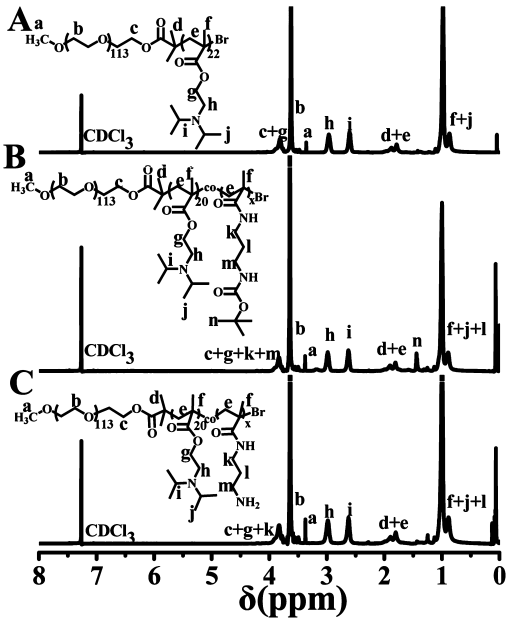

Figure 1. ^{1}H NMR spectra of (A) mPEG-*b*-PDPA, (B) mPEG-*b*-P(DPA-*co*-*Boc*-APA), (C) mPEG-*b*-P (DPA-*co*-APA) copolymers in $CDCl_3$-*d*.

chosen in this study was 5 kDa with 113 repeating units. Therefore, the repeating units of DPA and Boc-APA can be confirmed by integral area ratio of DPA units at 2.96 ppm (−O−CH_2−$\underline{CH_2}$-N-) and the Boc-APA unit at 1.45 ppm (N-(C═O)−O-C-($\underline{CH_3}$)) in comparation with the known EG unit (-$\underline{CH_2}$-$\underline{CH_2}$-O) at 3.65 ppm. The characteristic peak of -C($\underline{CH_3}$)$_3$ in Boc-APA units disappeared after the hydrolysis reaction, demonstrating that PEDPA copolymers were synthesized successfully. In addition, as shown in Figure 2, the narrow distribution all the four copolymers confirmed that the polymerization method and separation procedure were highly efficient.

CMC was an indispensable parameter of amphiphilic copolymers in drug delivery, which was related to the stability of NPs during the systemic circulation and drug release behavior.[29,30] The CMC value of PEDPA copolymers was measured by fluorescence spectroscopy using pyrene as fluorescence probe, which were favorably dissolved in the

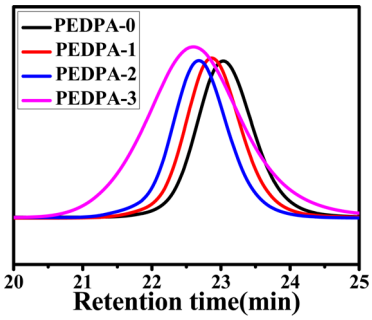

Figure 2. GPC chromatogram of PEDPA copolymers determined in THF at a flow rate of 1.0 mL/min.

hydrophobic core of NPs with dramatic variation of fluorescence spectra.[31] Figure S2A in the Supporting Information represents the typical emission spectrum of pyrene in PEDPA-3 copolymer solutions and Figure S2B in the Supporting Information shows the intensity ratio of I_{373}/I_{383} versus the logarithm of the concentration of PEDPA copolymers. As summarized in Table1, the CMC value of PEPDA copolymers was low and slightly increased with the increase of APA units, which may be attributed to the fact that the introduction of positively charged APA units decreased the hydrophobicity of PDPA chains. Hence, because of the low CMC value of PEDPA copolymers, the original morphology of PEDPA NPs was expected to be maintained during the systemic circulation.

3.2. Preparation of PEDPA/CAD NPs via synergetic electrostatic and hydrophobic interactions. First, the CAD prodrug was synthesized according to Park's study with some modifications,[32,33] which was confirmed by ^{1}H NMR and UV−visible spectroscopy (shown in Figure S3 in the Supporting Information). Then, the particle size, zeta potential, size distribution (PDI), and micromorphology of all the obtained NPs were measured by Zetasizer and TEM, respectively (as summarized in Table 2).

Obviously, DLC and DLE increased with the increase of amino groups, which was inferred that the two carboxyl groups in CAD molecule could form electrostatic interaction with amino groups on the PEDPA copolymer, cooperating with the hydrophobic interaction between CAD molecules and PDPA moieties to facilitate CAD loading. To verify the above assumption, we measured zeta potential of PEPDA/CAD NPs, which was slightly lower than that of blank PEPDA NPs, indicating the electrostatic interaction between CAD and PEPDA copolymer. Subsequently, in order to verify the hydrophobic interactions between PDPA segments and CAD molecules, the fluorescence emission spectrum of CAD and PEPDA/CAD NPs with the same CAD concentration was investigated. The excitation wavelength was set at 502 nm, which was the maximum absorption wavelength of CAD measured by UV−visible spectroscopy. As illustrated in Figure S4 in the Supporting Information, the fluorescence intensity of

DOI: 10.1021/acsami.5b00962
ACS Appl. Mater. Interfaces 2015, 7, 6340−6350

Table 2. Characterization of PEPDA and PEPDA/CAD NPs

	PEPDA NPs			PEPDA/CAD NPs				
sample	size (nm)[a]	ζ (mV)[a]	PDI[a]	size (nm)[a]	ζ (mV)[a]	PDI[a]	DLC (%)[b]	DLE (%)[b]
PEDPA-0	130 ± 2.2	−5.6 ± 0.05	0.12 ± 0.03	136 ± 3.3	−8.9 ± 0.05	0.13 ± 0.01	2.5 ± 0.3	17.1 ± 0.2
PEDPA-1	145 ± 3.4	−2.3 ± 0.03	0.14 ± 0.03	138 ± 4.7	−6.2 ± 0.04	0.12 ± 0.03	6.7 ± 0.5	44.7 ± 0.5
PEDPA-2	158 ± 4.8	4.1 ± 0.05	0.11 ± 0.02	145 ± 2.8	−3.9 ± 0.06	0.12 ± 0.02	10.1 ± 0.8	66.7 ± 0.8
PEDPA-3	164 ± 3.6	7.1 ± 0.02	0.13 ± 0.03	152 ± 3.9	−2.8 ± 0.05	0.14 ± 0.03	12.6 ± 0.6 0.2	84 ± 0.6

[a]Measured by Zetasizer. [b]Verified by UV−visible spectrum. The feeding ratio of CAD was 15%. The data were expressed as mean ± SD, n = 3.

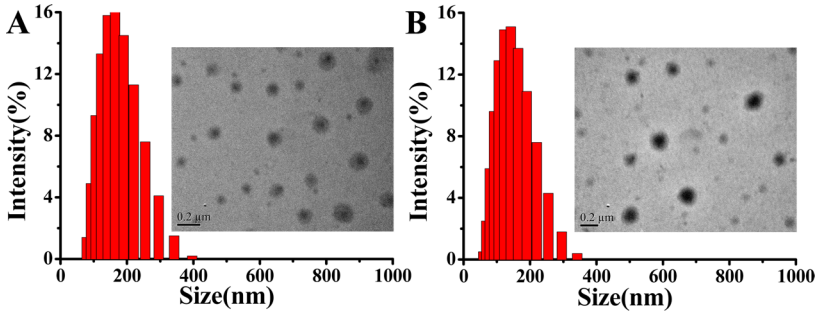

Figure 3. (A) Size distribution and morphology of PEDPA-3 NPs and (B) PEDPA-3/CAD NPs.

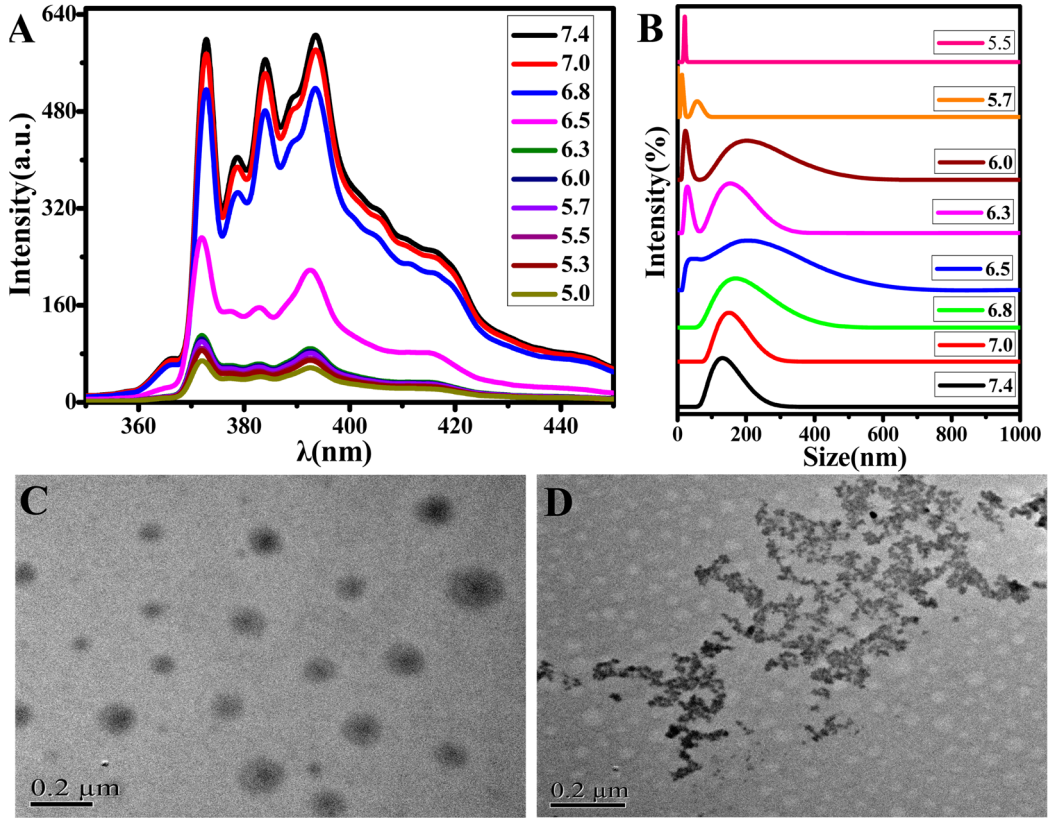

Figure 4. (A) Emission spectrum of pyrene and (B) change of particle size against pH; (C) micromorphology of PEDPA-3 NPs at pH 7.4 and (D) pH 5.0.

PEPDA-3/CAD NPs was much lower than that of free CAD, despite the concentration of CAD being the same. It was mainly due to the fact that CAD was encapsulated into the hydrophobic core of PEDPA NPs in the quenched state, which might be attributed to the collisional interactions between the aromatic molecules in the ground and excited states.[10,34] Furthermore, the difference of particle size and morphology between PEDPA-3 NPs and PEDPA-3/CAD NPs further validated the successful loading of CAD into PEDPA NPs. As shown in Figure 3, not only the size of PEDPA-3/CAD NPs was slightly smaller than PEDPA-3 NPs, but also the hydrophobic core of PEDPA-3/CAD NPs was more compacted than blank PEDPA-3 NPs, confirming that the CAD molecules were successfully encapsulated into the hydrophobic core in aggregated state. Importantly, all the PEDPA/CAD NPs exhibited excellent serum stability in the

DOI: 10.1021/acsami.5b00962
ACS Appl. Mater. Interfaces 2015, 7, 6340−6350

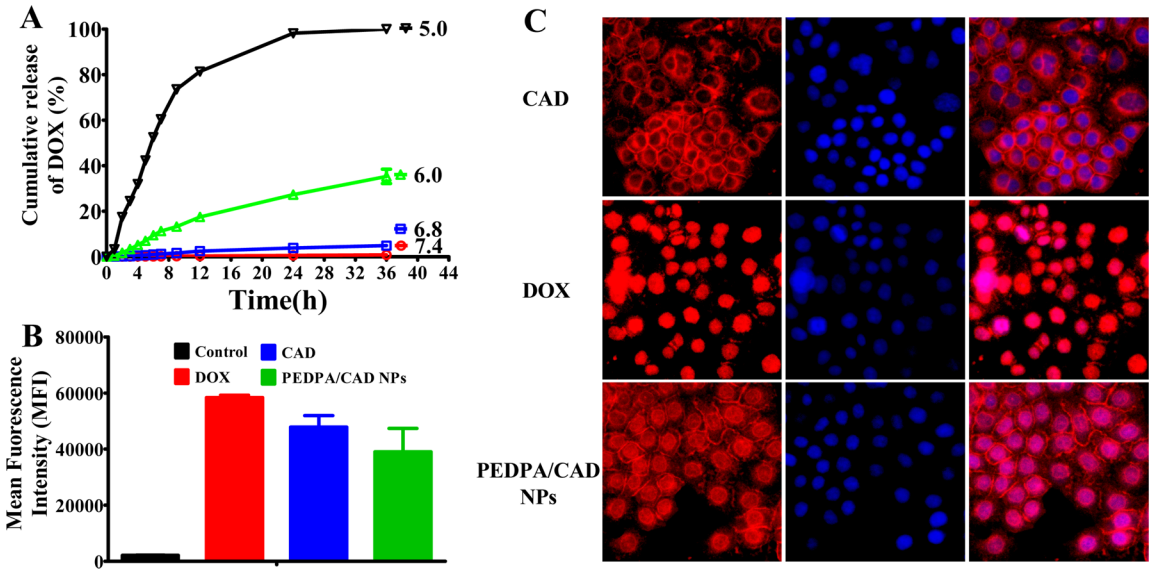

Figure 5. (A) In vitro DOX release from PEDPA-3/CAD NPs; (B) flow cytometry measurement of the amount of DOX and CAD intracellularly after incubation with CAD, PEDPA-3/CAD NPs, and free DOX for 4 h; (C) intracellular drug distribution after incubation with CAD, PEDPA-3/CAD NPs and free DOX for 4 h. For each panel, images from left to right show DOX fluorescence in cells (red) and cell nuclei stained by DAPI (blue) and overlays of two images. Error bars represent the standard deviation, $n = 3$.

presence of 10% FBS at pH 7.4 (shown in Figure S5 in the Supporting Information). Wherein, PEDPA-3/CAD NPs with favorable drug loading ability and stability was used in the following studies.

3.3. pH-Sensitivity of PEDPA NPs. To track the hydration condition against pH variation in the hydrophobic core, we took pyrene as the fluorescence probe because of its high responsiveness to the polarity change.[31] As shown in Figure 4A, the emission spectrum of pyrene as a function of pH was monitored. A sharp decrease in fluorescence intensity was observed at pH 6.5, indicating the remarkable polarity change encountering with pyrene, which demonstrated the partial hydration in the hydrophobic core of PEDPA-3 NPs due to the ionization of DPA units. Upon further lowering the pH to the p*K*a (~6.3) of DPA, the fluorescent intensity decreased approximately to the lowest point, which could be attributed to the fact that half of the DPA units were ionized at p*K*a value in principal, leading to the dramatic change of the ratio of the hydrophilic and hydrophobic from 1:1.4 to 2.4:1. Although further lowering the pH to 5.0, no obvious variation of fluorescent intensity and ratio of I_1/I_3 were observed. It was inferred that the NPs were significantly destabilized or disassembled because of the conformational transition of the polymer chains at p*K*a.

Meanwhile, the fluctuation of particle size against pH variation was evaluated. As shown in Figure 4B. the particle size increased slightly with pH decreasing from 7.4 to 6.8, which might be attributed to the fact that the electrostatic repulsion between positively charged amino groups impeded the compact assembly of hydrophobic core.[35] However, upon further decreasing the pH to 6.5, the particle size increased dramatically accompanying with considerable broad distribution, which was the same with that of pH 6.3 and 6.0. It could be explained by the fact that dramatic change in the ratio of the hydrophilic and hydrophobic because of the ionization of PDPA segments led to the significant change of assembly behavior.[36] Furthermore, the particle size could not even be detected at pH lower than 5.7, indicating that the NPs disassembled completely, which was consistent with the result of fluorescent measurement.

In addition, the change of morphological characteristics was measured by TEM (shown in Figure 4C, D). At pH 7.4, the core−shell structure of NPs was evident, however, random polymer aggregates were observed at pH 5.0, which indicated that the NPs were disintegrated and the copolymers were totally water-soluble. Therefore, the favorable pH-sensitivity of PEDPA NPs was significant for the acid-triggered intracellular anticancer drug release.

3.4. Cooperative pH-Sensitivity Triggered Drug Release Profile. The intracellular microenvironment of tumor cells was typically characterized by the slightly acid pH in the endosomal (5.0−6.0) and lysosomal (4.0−5.0) compartments.[21,37] Therefore, highly effective nanocarriers must give a sharp response to the subtle pH change between systemic circulation and tumor intracellular microenvironment. The acid-triggered charge reversal of CAD to DOX was studied by HPLC at scheduled time intervals.[32,38] As shown in Figure S6 in the Supporting Information, the hydrolysis of *cis*-aconityl linkage of CAD was clearly pH dependent. Approximately 4.2% free DOX was recovered after incubation for 24 h at pH 7.4. However, 51.3% of DOX was reconverted from CAD after 24 h at pH 6.0 and nearly 100% at pH 5.0, respectively. The result indicated that the pharmacological activity of DOX would be recovered in endo/lysosomal compartments due to the hydrolysis of *cis*-aconityl linkage in mildly acidic environment.

Subsequently, the release behavior of DOX from PEDPA-3/CAD NPs were conducted at pH 7.4, 6.8, 6.0, and 5.0, respectively, mimicking the pH gradient from blood circulation to the endo/lysosomal compartments. As shown in Figure 5A, about 2.5% of free DOX were released within 24 h at pH 7.4. However, approximately 20% of loaded DOX was released at pH 6.0 and nearly 80% at pH 5.0 within 12 h, respectively. The DOX release profile was clearly pH-dependent, owing to not only the gradual protonation of the PDPA block leading to the disassembly of PEDPA-3/CAD NPs, but also the accelerated hydrolysis of *cis*-aconityl linkage weakening the electrostatic

DOI: 10.1021/acsami.5b00962
ACS Appl. Mater. Interfaces 2015, 7, 6340−6350

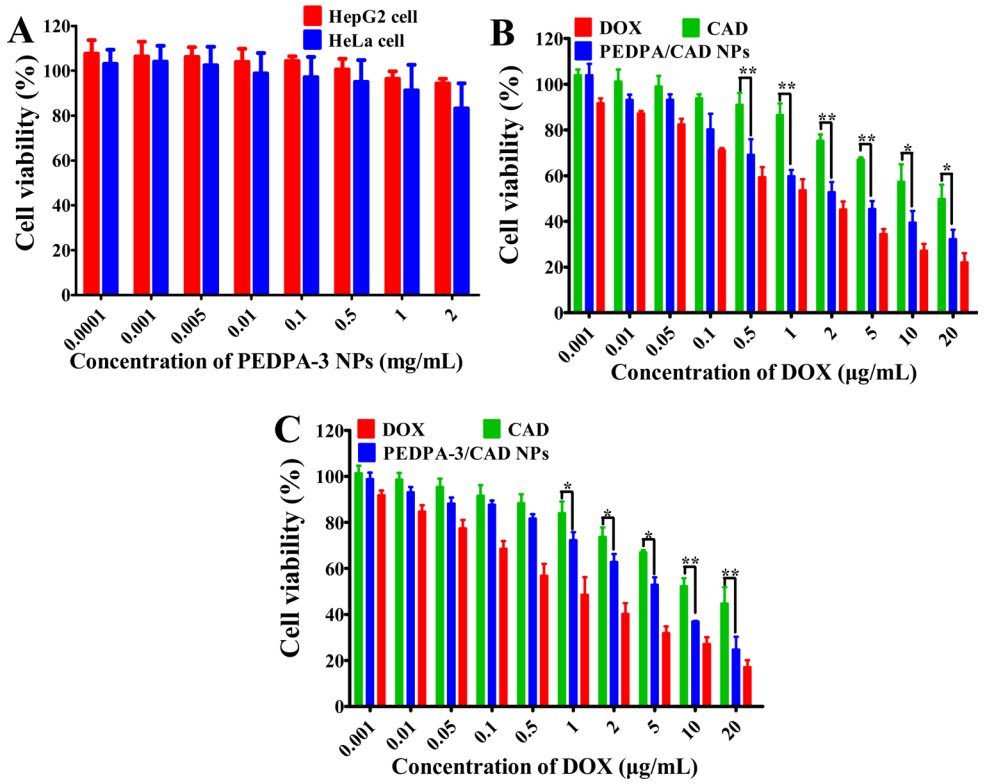

Figure 6. (A) Viability of HeLa and HepG2 cells after incubation with blank PEDPA-3 NPs for 48 h; (B) viability of HeLa and (C) HepG2 cells after incubation with CAD, PEDPA-3/CAD NPs, and free DOX for 48 h (*p < 0.05, **p < 0.01). Error bars represent the standard deviation (n = 6).

interaction between PEDPA-3 copolymers and CAD molecules, which should be beneficial for tumor treatment in vivo. Namely, DOX release from PEDPA-3/CAD NPs will be switched off during the systematic circulation (pH 7.4). However, prompt DOX release will be turned on upon entrapped in the endo/lysosomal compartments (pH 4.0−6.5) after endocytosis.

Then, the studies of endocytosis and drug release behavior of NPs formulations intracellularly were performed on flow cytometry and inverted fluorescence microscope. As shown in Figure 5B, fluorescence signals of DOX could be detected, indicating DOX, CAD and PEDPA-3/CAD NPs could be internalized by tumor cells. As being reported, free DOX mainly distributed in the cell nucleus with the strongest fluorescent intensity, since it was easy to enter into cells via passive diffusion.[39,40] However, the fluorescence intensity of CAD treated group was lower than free DOX, which may be attributed to the electrostatic repulsion between negative charged CAD molecule and cytomembrane. As shown in Figure 5C, the results of fluorescence microscope demonstrated that CAD mainly located in perinuclear areas instead of in the nucleus, which was in line with previously reported work as DOX derivatives were difficult to enter into the nucleus than free DOX.[41,42] However, significant fluorescent signal of DOX was detected in the nucleus after incubated with PEDPA-3/CAD NPs for 4 h, indicating that CAD delivered by PEDPA-3/CAD NPs could be released and reconverted into DOX induced by the cooperative pH-sensitivity property effectively.

3.5. In Vitro Antitumor Effect. To assess the antitumor effect of PEDPA-3/CAD NPs in vitro, we evaluated the cell biocompatibility of blank PEDPA-3 NPs and cytotoxicity-free DOX, CAD, and PEDPA-3/CAD NPs on HepG2 and HeLa cells. As shown in Figure 6A and Figure S7 in the Supporting Information, the blank PEDPA-3 NPs demonstrated good cytocompatibility. Figure 6B, C represent the viability of HeLa and HepG2 cells after being incubated with CAD, PEDPA-3/CAD NPs, and free DOX for 48 h, respectively, and the IC_{50} values are summarized in Table 3. The IC_{50} values of CAD for both cells are much higher than that of free DOX, indicating that the cytotoxicity of DOX could be significantly reduced via charge reversal modification. However, the PEDPA-3/CAD NPs exhibited markedly higher cytotoxicity than CAD against both the two cell lines, which was in line with the intracellular drug release studies, since the PEDPA-3/CAD NPs was able to release the load CAD efficiently accompanying with the acid-induced hydrolysis to reconvert the free DOX. It was also inferred that the encapsulation of CAD into PEDPA-3 NPs may resulted in enhanced treatment efficiency with potentially catabatic side effect in vivo.

Table 3. IC_{50} Value of CAD, PEDPA-3/CAD NPs, and Free DOX

	IC_{50} (μg/mL)	
sample	HepG2 cell	HeLa cell
free DOX	1.21	1.05
CAD	16.2	12.3
PEDPA-3/CAD NPs	3.25	4.82

3.6. In Vivo Animal Experiments. *3.6.1. Ex Vivo Imaging Studies.* The above results demonstrated that the PEDPA-3/CAD NPs had great potential in drug loading and intracellular release. However, nanocarriers must travel through the initial site of injection to the site of action, during which multiple

DOI: 10.1021/acsami.5b00962
ACS Appl. Mater. Interfaces 2015, 7, 6340−6350

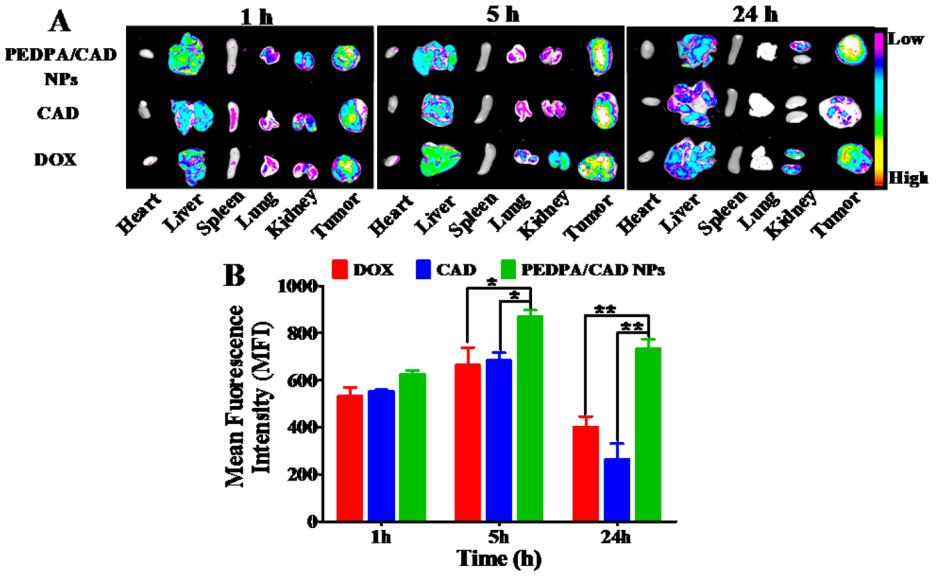

Figure 7. (A) Ex vivo imaging of tumor and major organs; (B) mean intratumoral fluorescent intensity of DOX (*p < 0.05, **p < 0.01). The data were expressed as mean ± SD, n = 3.

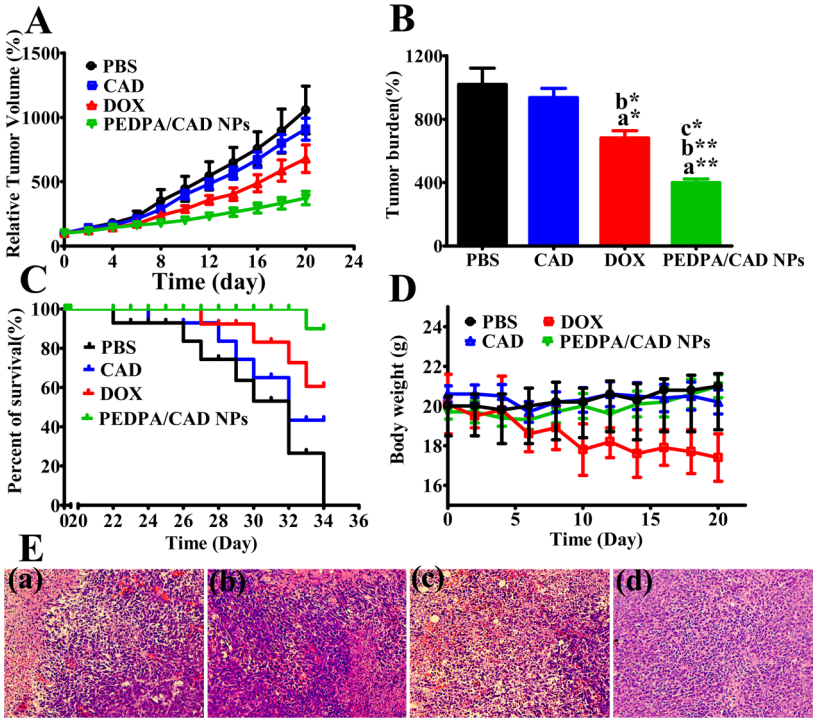

Figure 8. (A)Tumor growth inhibition of different formulations. (B) Comparation of tumor volume postinjection for 20 days (*p < 0.05, **p < 0.01. a = compared with negative control, b = compared with CAD, c = compared with free DOX). (C) Life span of the mice. (D) Relative body weight change after treatment. Error bars represent the standard deviation (n = 10). (E) Histopathological analysis of tumors in HepG2 tumor xenograft-bearing Balb/c mice: (a) DOX, (b) CAD, (c) PEDPA-3/CAD NPs, (d) saline, control.

biological barriers have to be circumvented.[43] To evaluate the drug distribution and accumulation in vivo, we injected free DOX, CAD, and PEDPA-3/CAD NPs intravenously into HepG2 tumor bearing Balb/c mice. Ex vivo fluorescence imaging showed the distribution of DOX in major organs and tumor tissues. As shown in Figure 7A, the intratumoral drug accumulation of PEDPA-3/CAD NPs was significantly higher than CAD and free DOX, which could be mainly attributed to the EPR effect.[8,44] Moreover, the excessive intratumoral interstitial fluid pressure would accelerate the clearance of free drugs that could not enter tumor cells.[45] Moreover, as summarized in Figure 7B, remarkably higher DOX fluorescent signal was detected post injection of PEDPA-3/CAD NPs for a longer time as 5 and 24 h. Obviously, the PEDPA-3/CAD NPs fabricated via synergistic electrostatic and hydrophobic interactions were able to facilitate the improvement of tumor accumulation through prolonging systemic circulation and tumor site retention, respectively.

3.6.2. In Vivo Antitumor Efficacy Evaluation. As shown in Figure 8A, the tumor volumes in the control group (PBS)

DOI: 10.1021/acsami.5b00962
ACS Appl. Mater. Interfaces 2015, 7, 6340−6350

increased rapidly and all drug treatment groups decreased tumor growth rates to various extent. As can be seen, the CAD treatment group exhibited no significant antitumor effect in comparation with control, which was in line with the results of cytotoxicity studies. The modification of DOX led to considerably reduced toxicity. However, treatment with the pH-sensitive PEDPA-3/CAD NPs resulted in the best therapeutic effect with highest survival rate, indicating CAD delivered by PEDPA-3/CAD NPs could be released and reconverted into DOX due to the cooperative pH-sensitivity property. Although the cytotoxicity of PEDPA-3/CAD NPs was lower than that of free DOX in vitro (shown in Figure 6), its treatment effect was significantly better in vivo.

To further confirm the antitumor efficacy of various DOX formulations, we randomly sacrificed three HepG2 tumor xenograft-bearing Balb/c nude mice in each group at the end of the treatment, and prepared the tumor sections for pathology analysis. The Cytoplasm and extracellular matrix were stained pink by eosin, and nucleus was stained blue by hematoxylin.[46,47] As shown in Figure 8E, all DOX formulations treated groups showed varying level of necrosis in comparation with PBS group, indicating that all DOX formats applied had antitumor effect to some extent. At the same dosage, the cell apoptosis of the CAD-treated group was lower than that of free DOX, indicating that the toxicity of DOX was reduced upon modification. However, PEDPA-3/CAD NPs treated group showed the most distinct damage to tumor tissues, as much nuclei absence and lack of discernible boundary regions were observed, and the above result was in line with in vivo tumor growth inhibition study.

3.6.3. Systemic Toxicity Evaluation. Systemic toxicity evaluation was indispensable for verifing the biosafety of the nanocarriers.[48,49] As shown in Figure 8D, the DOX treatment group demonstrated rapid body weight loss after injection, indicating that remarkable side effects were caused by DOX. In contrast, the mice treated with CAD and PEDPA-3/CAD NPs showed no obvious body weight fluctuation. In addition, as shown in Figure 9, histological analysis of major organ slices of

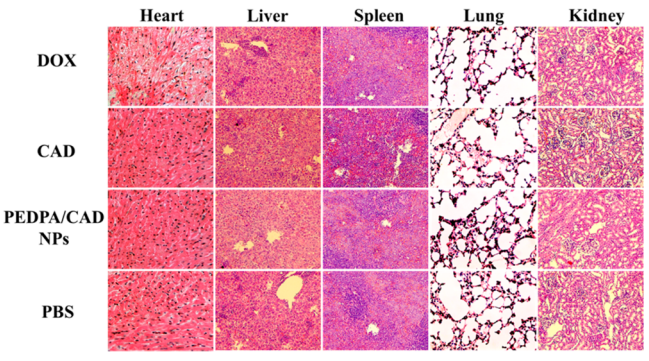

Figure 9. Histopathologic analysis of major organs after H&E staining, which were harvested from mice treated with DOX, CAD, PEDPA-3/CAD NPs, and saline on 20th day.

mice treated with saline, CAD, and PEDPA-3/CAD NPs exhibited no obvious tissue damage. However, in terms of DOX-treated group, notable cardiotoxicity was observed, which was characterized by flake myocardial degeneration in ventriculus sinister, myocardial swelling, cytoplasmic relaxation with small fat drops of cavitation, myofibril loose and nucleus degeneration. Therefore, these dramatic differences confirmed that the charge reversal modification of DOX and its encapsulation within PEDPA NPs via synergetic hydrophobic and electrostatic interactions decreased the exposure of DOX to the major organs and resulted in lower undesirable toxicities.

4. CONCLUSIONS

In this work, we demonstrated a kind of novel amphiphilic polyelectrolyte/prodrug nanoparticles for controlled DOX delivery, which was fabricated via synergistic electrostatic and hydrophobic interactions with cooperative pH-sensitivity. Notably, with polymer−drug synergetic noncovalent interactions, the drug loading content was significantly increased with favorable serum stability. Meanwhile, with cooperative pH-sensitivity, DOX could be released efficiently from the PEDPA-3/CAD NPs and exerted therapeutic action in cell nucleus, which led to commendable cytotoxicity against HeLa and HepG2 cells. In the HepG2 tumor xenograft-bearing Balb/c nude mice, the PEDPA-3/CAD NPs showed enhanced accumulation in tumor tissue, significantly higher antitumor effect, and lower side effect than free DOX. Consequently, this novel amphiphilic polyelectrolyte/prodrug NP designed in this work, which potentially resolved the extracellular stability versus intracellular drug release dilemma, would provide a promising nanomedicine platform for cancer therapy.

■ ASSOCIATED CONTENT

Ⓢ Supporting Information

^{1}H NMR spectra of mPEG-Br, fluorescence emission spectra of pyrene in PEDPA-3 copolymer solutions and plots of the intensity ratios of I_{383}/I_{373}, ^{1}H NMR spectra and UV−visible spectroscopy of CAD, fluorescence emission spectra of CAD and PEDPA-3/CAD NPs, serum stability studies of PEDPA/CAD NPs, hydrolysis rate of CAD under different pH, and viability of 3T3 cells and THP-1 cells after incubation with blank PEDPA-3 NPs for 48 h. This material is available free of charge via the Internet at http://pubs.acs.org.

■ AUTHOR INFORMATION

Corresponding Authors

*E-mail: kongdeling@nankai.edu.cn.
*E-mail: jhuazhang@tju.edu.cn.

Author Contributions

†P.H. and W.W. contributed equally to this work.

Notes

The authors declare no competing financial interest.

■ ACKNOWLEDGMENTS

This project was supported by the National Natural Science Foundation of China (31271073, 81301309, 31470925, 31470963, and 81171371).

■ REFERENCES

(1) Minotti, G.; Menna, P.; Salvatorelli, E.; Cairo, G.; Gianni, L. Anthracyclines: Molecular Advances and Pharmacologic Developments in Antitumor Activity and Cardiotoxicity. *Pharmacol. Rev.* **2004**, *56*, 185−229.

(2) Tewey, K. M.; Rowe, T. C.; Yang, L.; Halligan, B. D.; Liu, L. F. Adriamycin-Induced DNA Damage Mediated by Mammalian DNA Topoisomerase II. *Science* **1984**, *226*, 466−468.

(3) Gewirtz, D. A. A Critical Evaluation of the Mechanisms of Action Proposed for the Antitumor Effects of the Anthracycline Antibiotics Adriamycin and Daunorubicin. *Biochem. Pharmacol.* **1999**, *57*, 727−741.

DOI: 10.1021/acsami.5b00962
ACS Appl. Mater. Interfaces 2015, 7, 6340−6350

(4) Carvalho, C.; Santos, R. X.; Cardoso, S.; Correia, S.; Oliveira, P. J.; Santos, M. S.; Moreira, P. I. Doxorubicin: The Good, the Bad and the Ugly Effect. *Curr. Med. Chem.* **2009**, *16*, 3267−3285.
(5) Nicolas, J.; Mura, S.; Brambilla, D.; Mackiewicz, N.; Couvreur, P. Design, Functionalization Strategies and Biomedical Applications of Targeted Biodegradable/Biocompatible Polymer-Based Nanocarriers for Drug Delivery. *Chem. Soc. Rev.* **2013**, *42*, 1147−1235.
(6) Zhuang, J.; Gordon, M. R.; Ventura, J.; Li, L.; Thayumanavan, S.; Thayumanavan, S. Multi-Stimuli Responsive Macromolecules and their Assemblies. *Chem. Soc. Rev.* **2013**, *42*, 7421−7435.
(7) Duncan, R. The Dawning Era of Polymer Therapeutics. *Nat. Rev. Drug Discovery* **2003**, *2*, 347−360.
(8) Fang, J.; Nakamura, H.; Maeda, H. The EPR Effect: Unique Features of Tumor Blood Vessels for Drug Delivery, Factors Involved, and Limitations and Augmentation of the Effect. *Adv. Drug Delivery Rev.* **2011**, *63*, 136−151.
(9) Huang, P.; Song, H.; Wang, W.; Sun, Y.; Zhou, J.; Wang, X.; Liu, J.; Liu, J.; Kong, D.; Dong, A. Integrin-Targeted Zwitterionic Polymeric Nanoparticles with Acid-Induced Disassembly Property for Enhanced Drug Accumulation and Release in Tumor. *Biomacromolecules* **2014**, *15*, 3128−3138.
(10) Kwon, G.; Naito, M.; Yokoyama, M.; Okano, T.; Sakurai, Y.; Kataoka, K. Physical Entrapment of Adriamycin in AB Block Copolymer Micelles. *Pharm. Res.* **1995**, *12*, 192−195.
(11) Gao, Z.; Zhang, L.; Sun, Y. Nanotechnology Applied to Overcome Tumor Drug Resistance. *J. Controlled Release* **2012**, *162*, 45−55.
(12) Hoffman, A. S. The Origins and Evolution of "Controlled" Drug Delivery Systems. *J. Controlled Release* **2008**, *132*, 153−163.
(13) Hu, X.; Li, H.; Luo, S.; Liu, T.; Jiang, Y.; Liu, S. Thiol and pH Dual-Responsive Dynamic Covalent Shell Cross-Linked Micelles for Triggered Release of Chemotherapeutic Drugs. *Polym. Chem.* **2013**, *4*, 695−706.
(14) Van Nostrum, C. F. Covalently Cross-Linked Amphiphilic Block Copolymer Micelles. *Soft Matter* **2011**, *7*, 3246−3259.
(15) Chang, L.; Wang, W.; Huang, P.; Lv, Z.; Hu, F.; Zhang, J.; Kong, D.; Deng, L.; Dong, A. Photo-Crosslinked Poly (ethylene glycol)-*b*-Poly (ε-caprolactone) Nanoparticles for Controllable Paclitaxel Release. *J. Biomater. Sci., Polym. Ed.* **2013**, *24*, 1900−1921.
(16) Yan, J.; Ye, Z.; Chen, M.; Liu, Z.; Xiao, Y.; Zhang, Y.; Zhou, Y.; Tan, W.; Lang, M. Fine Tuning Micellar Core-Forming Block of Poly (ethylene glycol)-block-Poly (ε-caprolactone) Amphiphilic Copolymers Based on Chemical Modification for the Solubilization and Delivery of Doxorubicin. *Biomacromolecules* **2011**, *12*, 2562−2572.
(17) Zhu, Y.; Che, L.; He, H.; Jia, Y.; Zhang, J.; Li, X. Highly Efficient Nanomedicines Assembled *via* Polymer−Drug Multiple Interactions: Tissue-Selective Delivery Carriers. *J. Controlled Release* **2011**, *152*, 317−324.
(18) Tian, Y.; Bromberg, L.; Lin, S. N.; Alan Hatton, T.; Tam, K. C. Complexation and Release of Doxorubicin from its Complexes with Pluronic P85-b-Poly(acrylic acid) Block Bopolymers. *J. Controlled Release* **2007**, *121*, 137−145.
(19) Kim, S. H.; Tan, J. P.; Nederberg, F.; Fukushima, K.; Colson, J.; Yang, C.; Nelson, A.; Yang, Y. Y.; Hedrick, J. L. Hydrogen Bonding-Enhanced Micelle Assemblies for Drug Delivery. *Biomaterials* **2010**, *31*, 8063−8071.
(20) Chang, L.; Deng, L.; Wang, W.; Lv, Z.; Hu, F.; Dong, A.; Zhang, J. Poly (ethyleneglycol)-*b*-Poly (ε-caprolactone-co-γ-hydroxyl-ε-caprolactone) Bearing Pendant Hydroxyl Groups as Nanocarriers for Doxorubicin Delivery. *Biomacromolecules* **2012**, *13*, 3301−3310.
(21) Meng, F.; Cheng, R.; Deng, C.; Zhong, Z. Intracellular Drug Release Nanosystems. *Mater. Today* **2012**, *15*, 436−442.
(22) Mura, S.; Nicolas, J.; Couvreur, P. Stimuli-Responsive Nanocarriers for Drug Delivery. *Nat. Mater.* **2013**, *12*, 991−1003.
(23) Delplace, V.; Couvreur, P.; Nicolas, J. Recent Trends in the Design of Anticancer Polymer Prodrug Nanocarriers. *Polym. Chem.* **2014**, *5*, 1529−1544.
(24) Li, Y.; Liu, R.; Yang, J.; Ma, G.; Zhang, Z.; Zhang, X. Dual Sensitive and Temporally Controlled Camptothecin Prodrug Liposomes Codelivery of siRNA for High Efficiency Tumor Therapy. *Biomaterials* **2014**, *35*, 9731−9745.
(25) Huang, P.; Liu, J.; Wang, W.; Li, C.; Zhou, J.; Wang, X.; Deng, L.; Kong, D.; Liu, J.; Dong, A. Zwitterionic Nanoparticles Constructed with Well-Defined Reduction-Responsive Shell and pH-Sensitive Core for "Spatiotemporally Pinpointed" Drug Delivery. *ACS Appl. Mater. Interfaces* **2014**, *6*, 14631−14643.
(26) Huang, P.; Yang, C.; Liu, J.; Wang, W.; Guo, S.; Li, J.; Sun, Y.; Dong, H.; Deng, L.; Zhang, J. Improving the Oral Delivery Efficiency of Anticancer Drugs by Chitosan Coated Polycaprolactone-Grafted Hyaluronic Acid Nanoparticles. *J. Mater. Chem. B* **2014**, *2*, 4021−4033.
(27) Sun, Y.; Zou, W.; Bian, S.; Huang, Y.; Tan, Y.; Liang, J.; Fan, Y.; Zhang, X. Bioreducible PAA-g-PEG Graft Micelles with High Doxorubicin Loading for Targeted Antitumor Effect Against Mouse Breast Carcinoma. *Biomaterials* **2013**, *34*, 6818−6828.
(28) Guo, S.; Huang, Y.; Zhang, W.; Wang, W.; Wei, T.; Lin, D.; Xing, J.; Deng, L.; Du, Q.; Liang, Z.; Liang, X.-J.; Dong, A. Ternary Complexes of Amphiphilic Polycaprolactone-graft-Poly (N,N-dimethylaminoethyl methaaylate), DNA and Polyglutamic Acid-graft-Poly (ethylene glycol) for Gene Delivery. *Biomaterials* **2011**, *32*, 4283−4292.
(29) Tyrrell, Z. L.; Shen, Y.; Radosz, M. Fabrication of Micellar Nanoparticles for Drug Delivery through the Self-Assembly of Block Copolymers. *Prog. Polym. Sci.* **2010**, *35*, 1128−1143.
(30) Morton, S. W.; Zhao, X.; Quadir, M. A.; Hammond, P. T. FRET-Enabled Biological Characterization of Polymeric Micelles. *Biomaterials* **2014**, *35*, 3489−3496.
(31) Wilhelm, M.; Zhao, C. L.; Wang, Y.; Xu, R.; Winnik, M. A.; Mura, J. L.; Riess, G.; Croucher, M. D. Poly(styrene-ethylene oxide) Block Copolymer Micelle Formation in Water: a Fluorescence Probe Study. *Macromolecules* **1991**, *24*, 1033−1040.
(32) Yoo, H. S.; Lee, E. A.; Park, T. G. Doxorubicin-Conjugated Biodegradable Polymeric Micelles Having Acid-Cleavable Linkages. *J. Controlled Release* **2002**, *82*, 17−27.
(33) Yoo, H. S.; Park, T. G. Biodegradable Polymeric Micelles Composed of Doxorubicin Conjugated PLGA-PEG Block Copolymer. *J. Controlled Release* **2001**, *70*, 63−70.
(34) Choi, K. Y.; Yoon, H. Y.; Kim, J.-H.; Bae, S. M.; Park, R.-W.; Kang, Y. M.; Kim, I.-S.; Kwon, I. C.; Choi, K.; Jeong, S. Y.; Kim, K.; Park, J. H. Smart Nanocarrier Based on PEGylated Hyaluronic Acid for Cancer Therapy. *ACS Nano* **2011**, *5*, 8591−8599.
(35) Dayananda, K.; Kim, M. S.; Kim, B. S.; Lee, D. S. Synthesis and Characterization of MPEG-b-PDPA Amphiphilic Block Copolymer *via* Atom Transfer Radical Polymerization and its pH-Dependent Micellar Behavior. *Macromol. Res.* **2007**, *15*, 385−391.
(36) Hu, Y. Q.; Kim, M. S.; Kim, B. S.; Lee, D. S. Synthesis and pH-Dependent Micellization of 2-(Diisopropylamino)ethyl Methacrylate Based Amphiphilic Diblock Copolymers *via* RAFT Polymerization. *Polymer* **2007**, *48*, 3437−3443.
(37) Huh, K.; Kang, H.; Lee, Y.; Bae, Y. pH-Sensitive Polymers for Drug Delivery. *Macromol. Res.* **2012**, *20*, 224−233.
(38) Zhu, S.; Hong, M.; Tang, G.; Qian, L.; Lin, J.; Jiang, Y.; Pei, Y. Partly PEGylated Polyamidoamine Dendrimer for Tumor-Selective Targeting of Doxorubicin: The effects of PEGylation Degree and Drug Conjugation Style. *Biomaterials* **2010**, *31*, 1360−1371.
(39) Misra, R.; Sahoo, S. K. Intracellular Trafficking of Nuclear Localization Signal Conjugated Nanoparticles for Cancer Therapy. *Eur. J. Pharm. Sci.* **2010**, *39*, 152−163.
(40) Cho, H. J.; Yoon, I. S.; Yoon, H. Y.; Koo, H.; Jin, Y. J.; Ko, S. H.; Shim, J. S.; Kim, K.; Kwon, I. C.; Kim, D. D. Polyethylene Glycol-Conjugated Hyaluronic Acid-Ceramide Self-Assembled Nanoparticles for Targeted Delivery of Doxorubicin. *Biomaterials* **2012**, *33*, 1190−1200.
(41) Ding, J.; Shi, F.; Li, D.; Chen, L.; Zhuang, X.; Chen, X. Enhanced Endocytosis of Acid-Sensitive Doxorubicin Derivatives with Intelligent Nanogel for Improved Security and Efficacy. *Biomater. Sci.* **2013**, *1*, 633−646.

DOI: 10.1021/acsami.5b00962
ACS Appl. Mater. Interfaces 2015, 7, 6340−6350

(42) Chhikara, B. S.; Mandal, D.; Parang, K. Synthesis, Anticancer Activities, and Cellular Uptake Studies of Lipophilic Derivatives of Doxorubicin Succinate. *J. Med. Chem.* **2012**, *55*, 1500−1510.
(43) Nichols, J. W.; Bae, Y. H. Odyssey of a Cancer Nanoparticle: From Injection Site to Site of Action. *Nano Today* **2012**, *7*, 606−618.
(44) Li, Y.; Liu, R.; Yang, J.; Shi, Y.; Ma, G.; Zhang, Z.; Zhang, X. Enhanced Retention and Anti-Tumor Efficacy of Liposomes by Changing their Cellular Uptake and Pharmacokinetics Behavior. *Biomaterials* **2015**, *41*, 1−14.
(45) Heldin, C. H.; Rubin, K.; Pietras, K.; Ostman, A. High Interstitial Fluid Pressure - An Obstacle in Cancer Therapy. *Nat. Rev. Cancer* **2004**, *4*, 806−813.
(46) Yang, Y.; Pan, D.; Luo, K.; Li, L.; Gu, Z. Biodegradable and Amphiphilic Block Copolymer−Doxorubicin Conjugate as Polymeric Nanoscale Drug Delivery Vehicle for Breast Cancer Therapy. *Biomaterials* **2013**, *34*, 8430−8443.
(47) She, W.; Luo, K.; Zhang, C.; Wang, G.; Geng, Y.; Li, L.; He, B.; Gu, Z. The Potential of Self-Assembled, pH-Responsive Nanoparticles of mPEGylated Peptide Dendron−Doxorubicin Conjugates for Cancer Therapy. *Biomaterials* **2013**, *34*, 1613−1623.
(48) Shi, J.; Xiao, Z.; Kamaly, N.; Farokhzad, O. C. Self-Assembled Targeted Nanoparticles: Evolution of Technologies and Bench to Bedside Translation. *Acc. Chem. Res.* **2011**, *44*, 1123−1134.
(49) Bae, K. H.; Chung, H. J.; Park, T. G. Nanomaterials for Cancer Therapy and Imaging. *Mol. Cells* **2011**, *31*, 295−302.

DOI: 10.1021/acsami.5b00962
ACS Appl. Mater. Interfaces 2015, 7, 6340−6350